

# Effect of nanocrystalline and ultrafine grain sizes on the strain rate sensitivity and activation volume: fcc versus bcc metals

Q. Wei<sup>a,\*</sup>, S. Cheng<sup>b</sup>, K.T. Ramesh<sup>a</sup>, E. Ma<sup>b</sup>

<sup>a</sup> Department of Mechanical Engineering, Johns Hopkins University, Latrobe 200, Baltimore, MD 21218, USA

<sup>b</sup> Department of Materials Science and Engineering, Johns Hopkins University, Baltimore, MD 21218, USA

Received 8 January 2004; received in revised form 18 March 2004

## Abstract

Two of the key parameters that are useful for understanding the deformation kinetics in metals with ultrafine grain (UFG) and/or nanocrystalline (nc) microstructure are the strain rate sensitivity (SRS) of the flow stress and the flow stress activation volume. In this paper, we present experimental results from our in-house tests on UFG Cu, Fe and Ta, along with those available in literature, regarding the behavior of SRS and activation volume of UFG/nc metals with face-centered cubic (fcc) and body-centered cubic (bcc) structures. The UFG metals were produced via severe plastic deformation (SPD), and confirmed using transmission electron microscopy. Our own results, as well as those in the literature, indicate that the SRS of the UFG/nc fcc metals is elevated, whereas that of UFG/nc bcc metals is much reduced compared to their coarse-grained counterparts. These trends appear to hold independent of the processing routes used to refine the grain size and of the testing method employed. The activation volumes in UFG fcc and bcc metals also exhibit different behavior. We present discussions to explain the observed trends. The implications of these findings for plastic instability are also discussed for the two lattice structures.

© 2004 Elsevier B.V. All rights reserved.

**Keywords:** Strain rate sensitivity; Activation volume; Ultrafine microstructure; Nanocrystalline; Deformation mechanism; Plastic instability

## 1. Introduction

The plastic deformation behavior of metals, and the dependence on grain size ( $d$ ) in particular, has long been a subject of extensive research. There has been a resurgence of interest in this topic recently, due to the advent of ultrafine-grained (UFG,  $d < \sim 500$  nm) and nanocrystalline (nc,  $d < 100$  nm) materials [1,2]. New deformation mechanisms have been predicted in the nc grain size regime [3–8], especially those associated with grain boundary processes. The processes controlling plastic deformation in nc/UFG metals are therefore under intense investigation worldwide.

It is generally accepted that plastic deformation of metals is a thermally activated process, such that the shear strain rate  $\dot{\gamma}$  can be described by an Arrhenius-type equation [9–15]

$$\dot{\gamma} = \dot{\gamma}_0 \exp\left(\frac{-\Delta G(\tau^*)}{k_B T}\right), \quad (1)$$

where  $k_B$  is the Boltzmann constant,  $T$  is the absolute temperature, and the pre-exponential  $\dot{\gamma}_0$  includes the number of possible activation sites, the average shear strain per successful thermal fluctuation and the frequency of the vibration of the elemental unit involved in the thermal activation.  $\Delta G$  is the activation energy and is usually a strong function of the shear stress  $\tau^*$ , which is itself defined by  $\tau^* = \tau_a - \tau_\mu$  where  $\tau_a$  is the applied shear stress and  $\tau_\mu$  is the athermal internal stress stemming from long-range obstacles. For more general stress states, the shear stress  $\tau^*$  is replaced by the effective stress  $\tau_e = \sqrt{(1/2)S_{ij}S_{ij}}$ , with  $S_{ij}$  being the components of the deviatoric stress tensor, and the shear rate  $\dot{\gamma}$  is replaced by the work-conjugate effective plastic strain rate  $\dot{\gamma}^p$ .

Although experiments employing strain rate changes are very useful in revealing deformation mechanisms, there is very limited experimental data on the strain rate sensitive mechanical properties of nc/UFG metals [16–26]. A systematic study from coarse-grained conventional microstructures down to UFG/nc grain sizes would therefore be particularly useful. The primary material parameters of interest are the strain rate sensitivity and the activation volume for the flow stress.

\* Corresponding author. Tel.: +1-410-516-5162;

fax: +1-410-516-4316.

E-mail address: qwei@pegasus.me.jhu.edu (Q. Wei).

There are two closely inter-related definitions of strain rate sensitivity (SRS) in the literature. The first is the so-called physically based strain rate sensitivity  $S$  written as [29]

$$S = \frac{k_B T}{v^*} \quad (2)$$

Here  $v^*$  is the activation volume, which is defined in terms of the derivative of the activation enthalpy with respect to stress [13], i.e.,

$$v^* = - \left[ \frac{\partial \Delta H(\tau)}{\partial \tau} \right]_T = k_B T \left( \frac{\partial \ln \dot{\gamma}}{\partial \tau} \right)_T \quad (3)$$

In Eq. (3),  $\Delta H(\tau)$  is the activation enthalpy. A second definition of SRS (common in engineering) has the form of a rate sensitivity parameter  $m$  defined as

$$m = \frac{\partial \ln \tau}{\partial \ln \dot{\gamma}} \quad (4)$$

This measure of rate sensitivity is valid for any constitutive function (e.g., it is directly the strain rate exponent in the power law function:  $[\tau/\tau_0] = [\dot{\gamma}/\dot{\gamma}_0]^m$ ), and the value of  $m$  is an indicator of the strain rate response that is useful for technological evaluations and comparisons. The physically based strain rate sensitivity  $S$ , its “engineering” counterpart  $m$  and the activation volume  $v^*$  are related as follows:

$$m = \frac{S}{\tau} = \frac{k_B T}{\tau v^*} \quad (5)$$

An analysis of the thermal activation parameters,  $v^*$  and  $m$ , can shed light on the rate controlling mechanisms in the plastic deformation of metals [10–13]. In the following, we present such an analysis for metals with nc/UFG microstructure, in comparison with the behavior of coarse-grained metals. The differences in behavior observed between the lattice structures, fcc versus bcc, will be highlighted.

The data reported below from our own experiments are for an fcc metal (Cu) and two bcc metals (Fe and Ta) with UFG microstructure. The UFG grain size of the metals was achieved through severe plastic deformation (SPD) [30], i.e., equal channel angular pressing (ECAP) [31] and low temperature rolling. Tensile tests were performed with strain rate jumps to extract the  $v^*$  and  $m$  parameters. These experimental results are discussed in conjunction with those reported in the literature for UFG as well as nc metals to demonstrate general trends for fcc and bcc metals with grain sizes in the UFG/nc regime.

## 2. Experimental details

The grain sizes of the Cu, Fe and Ta samples were refined through four passes of ECAP via route C [32], which resulted in a UFG microstructure of an average grain size of  $\sim 300$  nm for Cu [33],  $\sim 300$  nm for Fe [34] and  $\sim 250$  nm for Ta [35], respectively. The total equivalent strain from

the ECAP procedure is  $\sim 4.46$  for each material [32]. As usual, route C produces UFG grains with elongated geometry and a large fraction of small-angle GBs [32]. To further refine the grain size, all three materials were rolled with a laboratory rolling miller. For Cu, the sample was immersed in liquid nitrogen before each rolling pass, and a total additional strain of  $\sim 1.18$ – $1.75$  was achieved. For Fe and Ta, rolling was conducted at room temperature, with a total additional strain of  $\sim 3.2$  for Fe and  $\sim 2.92$  for Ta, respectively. The materials that have been further cold rolled from the ECAP state will be referred to as ECAP + CR hereafter in this paper. Also, a Cu billet cut from an OFHC Cu block was rolled at liquid nitrogen temperature to a total strain of  $\sim 2.0$  (this material is referred to as cold-def henceforth). TEM samples of the processed materials were prepared using standard double jet techniques for microstructure observations.

Tensile samples were cut out from the processed materials using wire electric discharge machining (EDM). All of the samples were polished to a mirror finish. Mechanical tests were conducted using an Instron 5582 machine in the displacement control mode. During the test, strain rate changes were carried out by changing the cross-head speed. Only those data points in the steady-state plastic flow regime (after yielding but before necking of the specimen) are used.

## 3. Results

### 3.1. Microstructure of the SPD processed materials

TEM investigations of pure Cu after ECAP are well documented in the literature [33,36]. At room temperature, both the strength and microstructure are saturated when the number of ECAP passes exceeds  $\sim 2$  [33], and when an average grain size of  $\sim 300$  nm is reached. To further refine the grain size, dynamic recrystallization has to be suppressed by means of processing at a lower temperature, such as the cold rolling at cryogenic temperatures described above. The resulting grain size is approximately 200 nm, as discussed before in Ref. [37].

TEM observations of Fe and Ta processed by four passes of route C have also been published elsewhere [34,35]. Briefly, in both materials, grain refinement is significant, but grain boundaries are mainly of the small-angle varieties. The grain boundaries in the as-ECAPed state are easily discernible in bright field TEM images. However, further cold rolling to a large strain resulted in a heavily cold-worked microstructure for which the grain size is difficult to resolve without ambiguity in TEM. As an example, Fig. 1 displays the TEM bright field (a), center dark field (b) and selected area diffraction pattern (c) of Ta that was ECAP processed followed by rolling at room temperature. Again, even though some grains can be resolved using dark field imaging, it is difficult to determine an average grain/subgrain size. Our

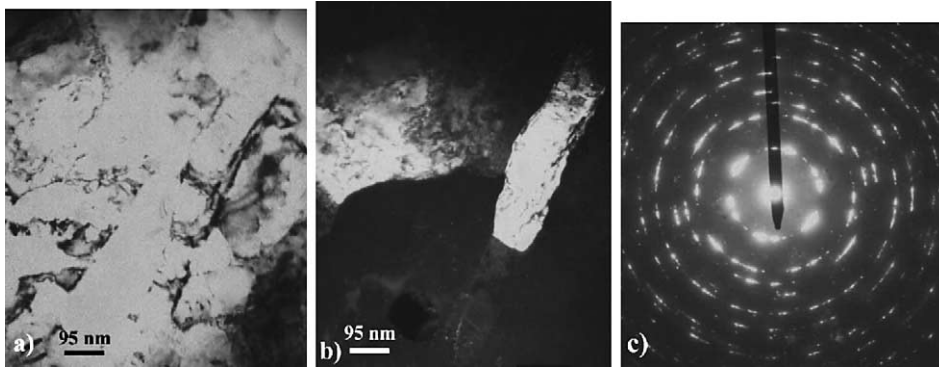


Fig. 1. TEM bright field (a), center dark field (b) and selected area diffraction pattern (c) of ECAP + RT rolled Ta. Texturing is evident from the concentrated {110} diffraction spots exhibiting a six-fold symmetry.

estimates of  $d$  for Fe and Ta are 200 nm and 150 nm respectively [34,35].

### 3.2. Mechanical testing results

Fig. 2(a) shows the stress–strain curves of the ECAP + CR Cu and the cold-def Cu. The rate-jump part (over the first 3% of plastic strains) of the stress–strain curves was re-plotted in Fig. 2(b) for clarity. We adopted up-jump (jump from a lower strain rate to a higher strain rate) in our experiments since a down-jump will exacerbate the effect from the machine compliance, and the interpretation of experimental

data becomes more involved [13]. In our experiments the strain rate is increased by a factor of 2 between consecutive rates.

The SRS and activation volume of the tested specimens were extracted from the jump test results. Fig. 2(c) shows a log–log plot of stress versus strain rate. The slopes of the linear fits give  $m = 0.015$  for the cold deformed Cu and  $m = 0.019$  for the ECAP + CR Cu, respectively. These values for  $m$  are in good agreement with those having similar microstructures reported in the literature [21,22]. Compared to large-grained Cu, the  $m$ 's of SPD processed UFG Cu have been substantially elevated ( $m$  of large-grained

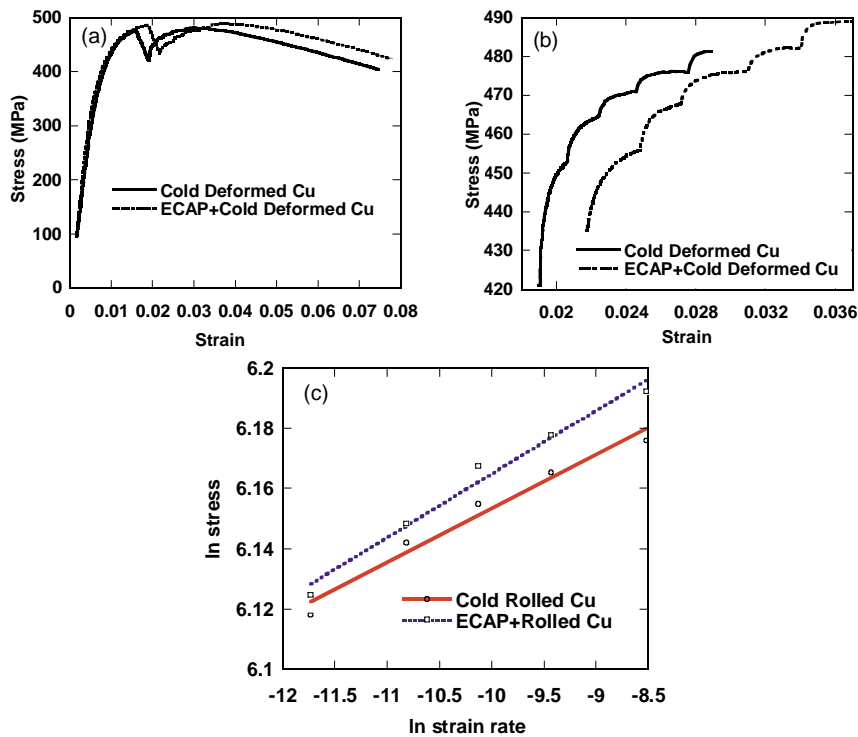


Fig. 2. Stress–strain curves (a) and the rate jump curves of SPD Cu (b). See text for details on determination of strain rate sensitivity and activation volume from the rate jump tests. A double logarithmic plot of stress vs. strain rate is displayed in (c), from which the strain rate sensitivities are extracted, with  $m = 0.015$  for the cold-deformed Cu and  $m = 0.019$  for the ECAP and cold rolled Cu, respectively.

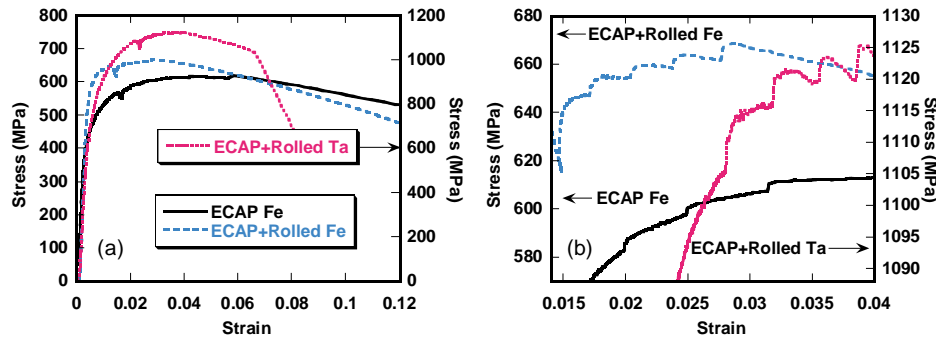


Fig. 3. Stress–strain curves (a) and the rate jump parts of the stress–strain curves (b) of SPD Fe and Ta. See text for determination of the strain rate sensitivity and activation volume from the rate jump tests.

fcc metals, including Cu, is around 0.004 [38]). The activation volume is obtained using Eq. (3). In keeping with common practice, the activation volume is expressed in terms of  $b^3$ , where  $b$  is the Burgers vector. Our results are  $\sim 48b^3$  for the cold-def Cu and  $\sim 41b^3$  for the ECAP + CR Cu, respectively. This is to be compared with the large activation volume, around  $1000b^3$ , for large-grained, un-deformed Cu. We will discuss the significance and possible implications of the much-increased  $m$  and drastically decreased activation volume in the SPD Cu in a subsequent section.

Fig. 3 displays the stress–strain curves of SPD Fe and Ta, with Fig. 3(b) focusing on the strain rate jump parts of the curves. The values of  $m$  derived are  $\sim 0.009$  for ECAP Fe, 0.007 for ECAP + CR Fe and 0.007 for ECAP + CR Ta, respectively, which are all considerably smaller than the  $m$  of large-grained Fe and Ta ( $\sim 0.045$  for Fe and 0.046 for Ta [34,35,38]). The activation volumes derived using Eq. (3) are  $\sim 26b^3$  for ECAP Fe,  $\sim 17b^3$  for ECAP + CR Fe and  $\sim 12b^3$  for ECAP + CR Ta.

In summary, rate jump tests in tension indicate that UFG Cu, a model fcc metal, exhibits substantially elevated strain rate sensitivity, about four times that of the large-grain structure; this is accompanied by a drastically reduced activation volume. On the other hand, for the two bcc metals, Fe and Ta, UFG microstructure leads to obviously reduced rate sensitivity. The experimentally derived activation volumes for UFG Fe and Ta are of the same order as that observed in large-grained bcc metals at very high stresses, i.e., around  $10b^3$  [13,29,38–40].

#### 4. Discussion

In this section, our experimental results will be discussed along with those reported in the literature. The focus is on a comparison of the effects of UFG/nc grain sizes on the SRS and activation volume in fcc and bcc metals. Finally, the implications of the SRS behavior for the onset of plastic instability under tension and compression will be briefly discussed.

##### 4.1. Summary of literature experimental data

Carreker and Hibbard [41] first reported the  $d$  dependence of  $m$  for tensile deformation of high-purity Cu. They observed that  $m$  increased slightly from 0.004 (large  $d$ ) to 0.0072 (small  $d$ ), but the  $d$  range studied was very small (12–90  $\mu\text{m}$ ). Early work on Ag and Cu also showed that polycrystalline samples had larger values of  $m$  than single crystals [38]. Coarse-grained Cu ( $d = 40 \mu\text{m}$ ) has an  $m$  of the order of 0.006 according to Follansbee et al. [42,43]. An  $m$  approaching 0.01 was reported for coarse-grained Cu deformed to large strains (high dislocation density) [44]. More recent studies of ultrafine-grained Cu showed elevated  $m$  [21,22,25,45]. A very large  $m$  (0.14) for Cu was quoted recently by Valiev et al. [25] for  $d \approx 100 \text{ nm}$  obtained using 16 passes of ECAP, though no test data were shown in their paper. We have measured before the  $m$  for a UFG Cu processed by ECAP + CR using load-reload compression tests so as to reach large plastic strains [6,45]. The tests yielded an  $m$  of 0.04, while a similar  $m$  (0.03) was obtained using the compressive flow stress data at a fixed strain of 15% but at different strain rates. The tensile jump tests shown in the preceding section gave  $m = 0.02$  for a similar ECAP + Cu (although processed separately). We therefore conclude that at  $d \approx 200 \text{ nm}$ ,  $m$  is at least 0.02 for Cu.

All of the data available for Cu are summarized in Fig. 4(a), including those from the literature. It is to be noted that the data point of Refs. [47,48] is from this lab, and that of [49] is from a conference paper. Although some inconsistency exists in the absolute values obtained by the different research groups, the data indicate a substantial increase in  $m$  when  $d$  is reduced into the UFG and nc regime, regardless of the technique used to process the material. The  $m$  has reached a level typical of the rate-sensitive bcc metals [38]. Also included in Fig. 4(b) are literature data for UFG/nc Ni, including ECAP Ni ( $d \approx 300 \text{ nm}$ ) [21] and electroplated nc Ni ( $d \approx 20\text{--}200 \text{ nm}$ ) [23,24]. For the yield strength of nc Ni, the  $m$  values reached 0.01–0.03 [23], again many times higher than for the coarse-grained counterpart ( $m \leq \sim 0.004$  [23,38]).

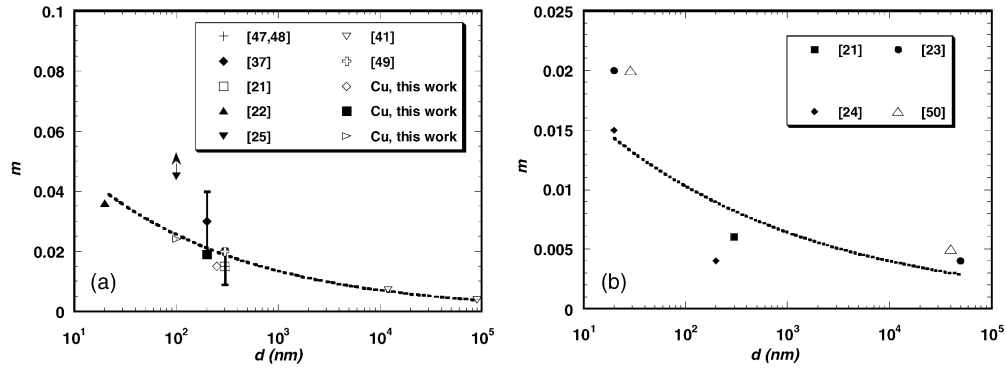


Fig. 4. Experimental results of  $m$  vs.  $d$  for Cu (a), and Ni (b). All the data show increased  $m$  with decreasing  $d$ . An unusually high  $m$  (0.14) quoted for a Cu ( $d = 100$  nm) in Ref. [25] is included with an arrow indicating that it is off scale in this plot. In (a), the data point corresponding to the hollow diamond is from the cold deformed Cu of this work, that to the black square is from the ECAP + cold deformed Cu of this work, and the hollow right triangle represents data from our in-house test of Cu particles in situ consolidated via ball milling. The dashed curves in the plots are for guide of eyes.

All the data above are obtained for deformation in the quasi-static and dynamic strain rate range. At creep rates, nc fcc metals Ni [20], Au [26] and Cu [46] all showed large  $m$  values greater than  $\sim 0.5$ , as obtained from the reciprocal of the stress exponent for steady-state creep. This is perhaps expected because, for the very slow strain rates observed under the applied stress, deformation can be entirely controlled by diffusional mechanisms such as Coble creep ( $m = 1$ ) and grain boundary sliding ( $m = 0.5$ ).

For bcc metals, we have reported before on UFG/nc Fe with  $d$  from 80 nm to 20  $\mu$ m [16]. There the samples were prepared by ball milling followed by a two-step consolidation process. The tests were performed under uniaxial compression. High-rate dynamic testing was conducted using the Kolsky bar technique [16]. By monitoring the flow stress at a fixed compressive strain for samples loaded at different strain rates (Fig. 5a), it was found that  $m$  decreases continuously with decreasing  $d$ , dropping by one order of magnitude at  $d = 80$  nm from  $m \approx 0.04$  for conventional Fe [38,51].

Such results are not unique to consolidated Fe. We have also measured the behavior of ECAP Fe ( $d \approx 300$  nm) un-

der compression. The results are shown in Fig. 5(b). The  $m$  value found for these ECAP Fe samples under compression with strain rate spanning a wide range (quasi-static to dynamic) is consistent with that found for the consolidated material at a similar  $d$ , and again obviously smaller than that of the coarse-grained Fe. These compression test results on Fe are consistent with the tensile test results reported in this paper.

The decreased  $m$  has also been observed under compressive loading for UFG-ECAP Ta ( $d$  of  $\sim 250$  nm [35]); the results are also included in Fig. 5(b). Again, this is consistent with the new tensile jump test data. Other bcc metals behave in a similar way. For example, an nc V was consolidated from ball-milled powders, using the same procedure as that for consolidated nc Fe [16]. The material has equiaxed grains and high-angle grain boundaries ( $d = 100$  nm) [52]. The compression test data have been included in Fig. 5(b). Summarizing all these results for bcc metals, we conclude from Fig. 5 that the  $m$  in UFG/nc bcc metals all decreased significantly from that of the annealed reference samples, independent of processing route and material. The values for

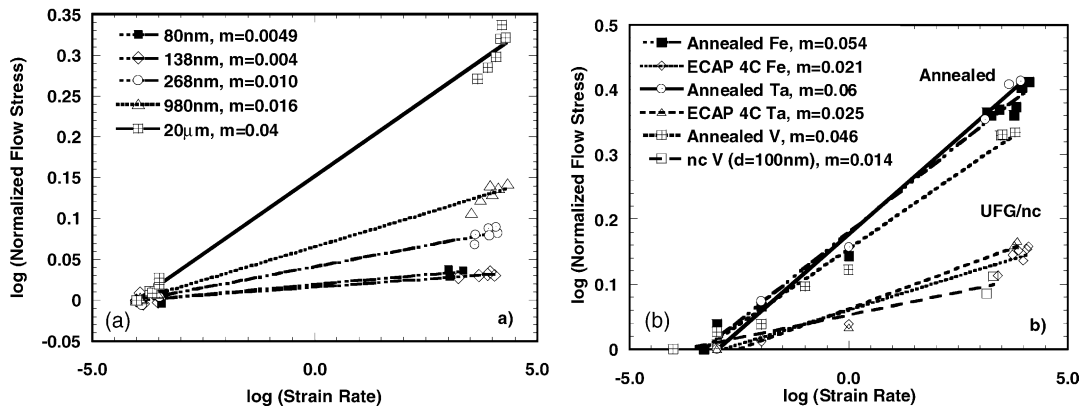


Fig. 5. Double logarithmic plot of normalized stress vs. strain rate to determine  $m$  for consolidated Fe with different grain sizes (80 nm–20  $\mu$ m) [16] (a). Double logarithmic plot of normalized flow stress vs. strain rate to determine  $m$  for ECAP Fe, ECAP Ta, and consolidated nc-V, in comparison with their annealed, coarse-grained counterparts (b).

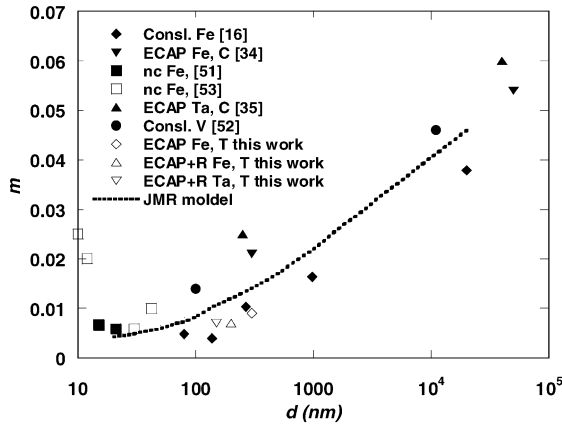


Fig. 6. Strain rate sensitivity  $m$  as a function of grain size for some bcc metals. Also included is the calculated curve (dashed line) using the JRM [16] model for bcc metals. The good agreement between the calculated curve and the experimental data is apparent. For those data points from literature, the references are given in the inset. A single letter C is used for “compression”, and T for “tension”.

$m$  of these bcc metals have dropped to approximate levels typical of conventional grain size fcc metals.

Fig. 6 summarizes the  $m$  as a function of  $d$  as extracted from Fig. 5 for these bcc metals in comparison with the values of their coarse-grained reference. Also included in Fig. 6 are the data of Malow et al. [51] for nc Fe also prepared using ball milling and consolidation. Their data are consistent with ours, e.g.,  $m \approx 0.006$  at  $d \sim 20$  nm. A recent nanoindentation experiment [53] on ball-milled Fe powder particles without consolidation, however, showed an unusual enhanced  $m$  for  $d < \sim 10$  nm (see Fig. 6). However, some uncertainties have to be resolved, with regard to the testing method on powder samples and the unusually low  $m$  (0.006) they obtained for their as-received, coarse-grained Fe.

#### 4.2. Explanations of the observed trends

We begin our discussion with the fcc metals. The survey above clearly indicates that for fcc metals, refined grain size down into UFG/nc regimes results in elevated SRS. For coarse-grained fcc metals, the primary obstacles to the motion of glissile dislocations is known to arise from forest dislocations, leading to the rate dependence of flow stress through thermal activation. According to the work of Becker [10,11,54], the activation volume can be written as

$$v^* = b \times \xi \times l^*, \quad (6)$$

where  $b$  is the Burgers vector of the dislocations,  $\xi$  is the distance swept out by the mobile dislocation during one activation event, and  $l^*$  is the length of dislocation segment involved in the thermal activation (or the Friedel sampling length that scales with the average contact distance between two obstacles). For large-grain fcc metals with forest cutting as the dominant mechanism for plastic deformation,  $l^*$  is roughly the average forest spacing which scales with the for-

est density  $\rho_f^{-1/2}$ , or following Taylor’s relation, with  $\mu b/\tau$ .  $\xi$  may also decrease slightly with increased applied stress [50,55]. It thus follows that the Becker activation volume would decrease with applied stress. As an example, for heavily deformed Cu,  $v^*$  can be decreased to as low as  $\sim 100b^3$  [56] (note that the  $v^*$  found in our experiments is outside the normal range and below the lower bound found for heavily cold-worked Cu). Combining Eqs. (5) and (6) we have

$$m = \frac{k_B T}{\tau \times v^*} = \frac{k_B T}{\tau \times l^* \times \xi \times b}, \quad (7)$$

in which  $\xi$  is roughly approximated to be constant. Therefore, the variation of  $m$  has to be understood from the combined variation of  $\tau \times l^*$ . We expect that the flow stress has contributions arising from both grain boundaries and dislocations, and it can be written as

$$\tau = \tau_0 + \left( \alpha \sqrt{\rho} + \frac{\beta}{\sqrt{d}} \right), \quad (8)$$

where the first term accounts for the lattice friction, the second arises from the Taylor contribution, and the third arises from the Hall-Petch relation.  $\alpha$  and  $\beta$  are retained as proportionality factors. The obstacle spacing or “sampling length”  $l^*$  can be viewed as having two possible limits,  $l_1^*$  and  $l_2^*$ :

$$l_1^* = \frac{a}{\sqrt{\rho}}, \quad (9)$$

$$l_2^* = \chi d$$

where  $l_1^*$  is likely to be the controlling length scale when the grain sizes and dislocation densities are large, and  $l_2^*$  is likely to be the controlling length scale at very small grain sizes (and small dislocation densities);  $a$  and  $\chi$  are proportionality factors. Thus, one anticipates that as the grain size is decreased there is a transition grain size when the controlling sampling length changes from  $l_1^*$  to  $l_2^*$ . A crude estimate of the transition size can be obtained by asking when  $l_1^*$  and  $l_2^*$  are of the same order of magnitude, and assuming that  $a$  and  $\chi$  are of the same order:  $d_{\text{transition}} \approx 1/\sqrt{\rho}$ . Using typical dislocation densities in metals, one estimates that  $d_{\text{transition}}$  is of the order of 10–500 nm. At conventional grain sizes we know that the forest cutting is dominant, so that we have

$$\tau \times l^* \cong \tau \times l_1^* = \left( \tau_0 + \alpha \sqrt{\rho} + \frac{\beta}{\sqrt{d}} \right) \left( \frac{a}{\sqrt{\rho}} \right) \cong \alpha a + \frac{a\beta}{\sqrt{\rho d}} \quad (10)$$

It follows that

$$m = \frac{k_B T}{\xi b} \frac{1}{\alpha a + a\beta/\sqrt{\rho d}} \quad (11)$$

In writing (10), the lattice friction term has been dropped since it is usually very small for fcc metals [57]. Eq. (11) indicates that when the dislocation density is increased (e.g., by large deformations) in a metal with a given  $d$ , the SRS

should increase (this change is not expected to be very large because at large grain sizes the second term in the denominator in Eq. (11) is relatively small). This explains the observations reported by Zehetbauer and Seumer [44].

On the other hand, as the grain size is refined into the UFG/nc regime, the controlling sampling length may become  $l_2^*$ , and we have

$$\begin{aligned} \tau \times l^* &\cong \tau \times l_2^* = \left( \tau_0 + \alpha\sqrt{\rho} + \frac{\beta}{\sqrt{d}} \right) \cdot \chi d \\ &\cong \chi\alpha\sqrt{\rho}d + \beta\chi\sqrt{d}, \end{aligned} \quad (12)$$

and now

$$m = \frac{k_B T}{\xi b} \frac{1}{\chi(\alpha\sqrt{\rho}d + \beta\sqrt{d})} \quad (13)$$

Eq. (13) indicates that when the grain size is refined into the UFG/nc regime,  $m$  should increase with reduced grain size. This explains the data from our in-house experiments as well as those from the literature, as displayed in Fig. 4. In this case, as  $d$  is reduced to below the transition size, forest dislocation density in the grain interior is expected to become very low [58], whereas the obstacle density associated with grain boundaries becomes very high. It is thus possible that the controlling intersection obstacles are the grain or subgrain boundaries, which predicated the derivation of Eq. (13).

For nc fcc metals, for low stresses an increased  $m$  is also expected from a constitutive response function [59–62] such as

$$\dot{\epsilon} = \frac{d_0}{d} \exp\left(-\frac{U}{k_B T}\right) \sinh\left(\frac{\sigma v^*}{k_B T}\right), \quad (14)$$

where  $U$  is the activation energy. As pointed out in [59,61], in the case of high temperature and low stress (creep), the stress and strain rate have a linear relation ( $m$  is thus unity). For high stresses, the Arrhenius relation of Eq. (1) applies. In either case, the SRS derived from this equation should be much larger than that of the large-grain fcc metals, and the activation volume should be that corresponding to atomic diffusion in the boundary, i.e., of the order of an atomic volume,  $\sim 1b^3$ , much smaller than observed in the experimental results presented earlier. Eq. (14) is based on the assumption of shear in grain boundary with no contribution to plasticity from the grain interior, and is thus applicable only to grain size below a certain value, usually below 20 nm for Cu, Ni and Au [60–62]. Our grain sizes are much larger and our measured  $m$  and  $v^*$  values suggest that this mechanism is unlikely.

Conrad [63] also proposed a model for Cu with UFG (10 nm–1000 nm) microstructure. Although the model would show the correct trends as well ( $m$  increasing with decreasing  $d$ ), his response function is derived again based on thermally activated shear of individual atoms inside the grain boundary, but in this case promoted by stress concentration due to the “pile-up” of dislocations at the

grain boundaries [63]. The predicted  $v^*$  of  $1b^3$  is again inconsistent with our experimental findings.

For small nc  $d$ , for example, in electroplated nc Ni ( $d \sim 30$  nm) [50], dislocations may not be available unless generated from the grain boundaries [64,65]. This defect-assisted heterogeneous process may become the rate-limiting step, rather than the gliding of mobile dislocations cutting through obstacles. However, the obstacle spacing ( $l^*$ ) discussed above in our model can in this case again be viewed as the source length for a dislocation generated into the lattice from the grain boundaries (the  $v^*$  may become very small, of the order of  $10b^3$ , in this case [50]). With this substitution, the general trend predicted by Eq. (13) remains valid.

The grain size dependence of the rate sensitivity of bcc metals, with a trend opposite to the fcc metals, is discussed next. In normal bcc metals, the peculiar non-planar dislocation core results in a very large Peierls-Nabarro stress at low homologous temperatures, which renders the yield and flow stress of single crystal or large-grain polycrystalline bcc metals rate and temperature sensitive [57]. The physical picture of Eq. (6) in bcc metals is closely associated with the kink-pair nucleation mechanism at the early stage of plastic deformation where contribution from edge dislocation can be neglected. This thermally activated process in the lattice is expected to remain the rate-limiting step for a wide range of grain sizes (atomistic simulation of energetics of motion of screw dislocations in Fe at finite temperature [66] indicated at a stress of 720 MPa, the critical kink-span is about  $4b$ , implying that the critical process is still kink nucleation controlled.). Here the term  $l^*$  can be understood to be the critical span between the two kinks in a kink pair [66], and  $\xi$  related to a critical unzipping distance for a screw dislocation which is a function of the junction strength [67]. The critical span is a decreasing function of the applied stress, following an inverse square root dependence and leveling off at very large applied stress, while the value of  $\xi$  should be roughly constant at a given temperature [67].

From Eq. (7),  $\tau v^*$  would again be the decisive factors for the SRS of bcc metals. The behavior of  $v^*$  discussed in the preceding paragraph thus predicts an increasing SRS with stress. In fact,  $v^*$  levels off quickly with the applied stress and SRS should then scale inversely with  $\tau$ , which should follow the Hall-Petch relation for the effect of grain size  $d$ . As a consequence, one should expect a reduced  $m$  with refined grain size, as observed in experiments (Figs. 5 and 6). The  $v^*$  derived in our tests are of the same order of magnitude as that typical for bcc metals at very large stresses, consistent with the notion that the same activation process persists in UFG bcc metals. This conclusion is also supported by calculations using a constitutive equations established for bcc metals, Ref. [16]. The result (dashed line in Fig. 6) compares favorably with experimental results in terms of the grain size effect on strain rate sensitivity. It becomes evident that, with the same Peierls barrier unchanged, the additive athermal contribution to the yield and flow stress due to Hall-Petch strengthening will become larger and larger as the grain size

is reduced, rendering UFG bcc metals less rate sensitive. The behavior of nc bcc metals with  $d$  much smaller than 100 nm is uncertain at present, due to limited data [53].

#### 4.3. Implications for plastic instability

For UFG/nc bcc metals, the reduced  $m$  should aggravate plastic instability. This has been demonstrated by shear localization in several UFG/nc bcc metals under either quasi-static or dynamic compression [16,28,34,35,51,52,68–71], including the Fe, V, Ta discussed in this paper. Such an instability may be less likely for fcc UFG/nc metals. Common to both fcc and bcc metals when  $d$  is reduced to the UFG/nc regime are the dramatic elevation in strength and the diminishing strain hardening capacity [7,16,17,28,58,68–72], both of which serve as destabilizing factors that may render the material susceptible to localized deformation [27,34]. But the opposite rate sensitivity behavior may also play a role. Another difference lies in the temperature dependence of  $m$  [38,73]. The  $m$  of fcc metals usually increases monotonically with  $T$ , as the flow stress decreases with temperature (cf. Eqs. (7) and (5)); whereas the  $m$  of bcc metals decreases with increasing  $T$  near RT. This phenomenon can be understood in light of the discussions in Section 4.2 (and Ref. [57]). Below a critical temperature the rate controlling process in bcc metals is solely due to the screw dislocations. Above it, the plastic behavior of bcc metals becomes more and more similar to that of fcc metals, i.e., the metals become less and less rate dependent. Above the athermal temperature  $T_a$ , bcc metals behave much the same as fcc metals.

### 5. Summary remarks

We have carried out tensile testing on UFG fcc Cu, and UFG bcc Ta and Fe. In particular, strain rate jump tests were performed to obtain strain rate sensitivity and activation volume of the three UFG metals. We found that, in accordance with experimental results obtained in other materials and through different techniques, the strain rate sensitivities of the UFG fcc metals is much elevated, and those of the UFG bcc metals much reduced compared to the coarse-grained microstructure. We also observed that the activation volume in UFG Cu has been reduced to such a level that forest cutting mechanism might not be able to account for the rate controlling process, whereas that of bcc metals remains largely unchanged in the UFG regime. We have presented a preliminary model for the thermally activated dislocation processes in fcc metals. The model is successful in explaining the trend observed for the available data for UFG/nc Cu and UFG/nc Ni. On the other hand, the behavior of UFG bcc metals may be explained using the kink-pair mechanism in much the same way as for coarse-grained microstructure. Here the increased Hall-Petch effect with decreased grain size renders the bcc metals less rate sensitive. While this reduced strain

rate hardening in UFG bcc microstructures, together with the much elevated strength and diminished work hardening ability, makes the material more prone to plastic instability [16,28,34,35,51,52,68–71], it may have beneficial effects on materials whose application requires enhanced plastic instability (e.g., kinetic energy penetrators).

### Acknowledgements

The authors thank Dr. T.W. Wright for helpful discussions. This work was performed under the auspices of the Center for Advanced Metallic and Ceramic Systems (CAMCS) at the Johns Hopkins University. This research was sponsored by the U.S. Army Research Laboratory under (ARMAC-RTP) and was accomplished under the ARMAC-RTP Cooperative Agreement No. DAAD19-01-2-0003. The views and conclusions contained in this document are those of the authors and should not be interpreted as representing the official policies, either expressed or implied, of the Army Research Laboratory or the U.S. Government. The U.S. Government is authorized to reproduce and distribute reprints for Government purposes not withstanding any copyright notation hereon.

### References

- [1] J.R. Weertman, D. Farkas, et al., MRS Bull. 24 (1999) 44.
- [2] K.S. Kumar, H. Van Swygenhoven, S. Suresh, Acta Mater. 51 (2003) 5743.
- [3] Y. Yamakov, D. Wolf, S.R. Phillpot, A.K. Mukherjee, H. Gleiter, Nat. Mater. 1 (2002) 45.
- [4] J. Schiøtz, E.D. Di Tolla, K.W. Jacobsen, Nature 391 (1998) 561.
- [5] A. Hasnaoui, H. Van Swygenhoven, P.M. Derlet, Science 300 (2003) 1550.
- [6] Y. Wang, M. Chen, F. Zhou, E. Ma, Nature 419 (2002) 912.
- [7] M. Chen, E. Ma, K. Hemker, H. Sheng, Y. Wang, X. Cheng, Science 300 (2003) 1275.
- [8] X.Z. Liao, F. Zhou, E.J. Lavernia, S.G. Srinivasan, M.I. Baskes, D.W. He, Y.T. Zhu, Appl. Phys. Lett. 83 (2003) 632.
- [9] U.F. Kocks, A.S. Argon, M.F. Ashby, Prog. Mater. Sci. 19 (1975) 1.
- [10] H. Conrad, J. Metals 16 (1964) 582.
- [11] J.W. Cahn, Nabarro FRN. Phil. Mag. A 81 (2001) 1409.
- [12] F.R.N. Nabarro, Phil. Mag. A 83 (2003) 3407.
- [13] G. Taylor, Prog. Mater. Sci. 36 (1992) 29.
- [14] N.F. Mott, Phil. Mag. 44 (1953) 742.
- [15] B. de Meester, C. Yin, M. Doner, H. Conrad, in: Rate Processes in Plastic Deformation of Materials-International Symposium on Rate Processes in Plastic Deformation, ASM, Cleveland, OH, 1975.
- [16] D. Jia, K.T. Ramesh, E. Ma, Acta Mater. 51 (2003) 3495.
- [17] D. Jia, K.T. Ramesh, E. Ma, Scr. Mater. 42 (2000) 73.
- [18] D. Jia, K.T. Ramesh, E. Ma, L. Lu, K. Lu, Scr. Mater. 45 (2001) 613.
- [19] D. Jia, Y.M. Wang, K.T. Ramesh, E. Ma, Y.T. Zhu, R.Z. Valiev, Appl. Phys. Lett. 79 (2001) 611.
- [20] N. Wang, Z. Wang, K.T. Aust, U. Erb, Mater. Sci. Eng. A 237 (1997) 150.
- [21] G.T. Gray, T.C. Lowe, C.M. Cady, R.Z. Valiev, I.V. Alexandrov, Nanostruc. Mater. 9 (1997) 477.
- [22] L. Lu, S.X. Li, K. Lu, Scr. Mater. 45 (2001) 1163.

- [23] F.D. Torre, H.V. Swygenhoven, M. Victoria, *Acta Mater.* 50 (2002) 3957.
- [24] R. Schwaiger, B. Moser, M. Dao, N. Chollacoop, S. Suresh, *Acta Mater.* 51 (2003) 5159.
- [25] R.Z. Valiev, I.V. Alexandrov, Y.T. Zhu, T.C. Lowe, *J. Mater. Res.* 17 (2002) 5.
- [26] H. Tanimoto, S. Sakai, H. Mizubayashi, *Nanostruc. Mater.* 12 (1999) 751.
- [27] T.W. Wright, *The Physics and Mathematics of Adiabatic Shear Bands*, Cambridge University Press, 2002.
- [28] Q. Wei, D. Jia, E. Ma, K.T. Ramesh, *Appl. Phys. Lett.* 81 (2002) 1240.
- [29] M. Tang, L.P. Kubin, G.R. Canova, *Acta Mater.* 46 (1998) 3221.
- [30] T.C. Lowe, R.Z. Valiev (Eds.), *Investigation and Application of Severe Plastic Deformation*, Nato Sci. Ser., vol. 80, Kluwer Academic Publishers, 2000.
- [31] V.M. Segal, *Mater. Sci. Eng. A* 197 (1995) 157.
- [32] M. Furukawa, Z. Horita, M. Nemoto, T.G. Langdon, *J. Mater. Sci.* 36 (2001) 2835.
- [33] S. Ferrasse, V.M. Segal, et al., *Metal. Mater. Trans. A* 28 (1997) 1047.
- [34] Q. Wei, L. Kecskes, T. Jiao, K.T. Hartwig, E. Ma, K.T. Ramesh, *Acta Mater.* 52 (2004) 1859.
- [35] Q. Wei, T. Jiao, S.N. Mathaudhu, E. Ma, K.T. Hartwig, K.T. Ramesh, *Mater. Sci. Eng. A* 358 (2003) 266.
- [36] W.H. Huang, C.Y. Yu, P.W. Kao, C.P. Chang, *Mater. Sci. Eng. A* 366 (2004) 221.
- [37] Y.M. Wang, E. Ma, *Mater. Trans.* 44 (2003) 1926.
- [38] H. Conrad, in: V.F. Zackey (Eds.), *High-Strength Materials*, Wiley, 1965.
- [39] S. Nemat-Nasser, W. Guo, M. Liu, *Scr. Mater.* 40 (1999) 859.
- [40] D. Brunner, V. Glebovsky, *Mater. Lett.* 44 (2000) 144.
- [41] R.P. Carreker Jr., W.R. Hibbard Jr., *Acta Metal.* 1 (1953) 656.
- [42] P.S. Follansbee, G. Regazzoni, U.F. Kocks, *Inst. Phys. Conf.* 70 (1984) 71.
- [43] P.S. Follansbee, U.F. Kocks, *Acta Mater.* 36 (1988) 81.
- [44] M. Zehetbauer, V. Seumer, *Acta Metal.* 41 (1993) 577.
- [45] Y.M. Wang, E. Ma, M.W. Chen, *Appl. Phys. Lett.* 80 (2002) 2395.
- [46] B. Cai, Q.P. Kong, L. Lu, K. Lu, *Scr. Mater.* 14 (1999) 755.
- [47] Y.M. Wang, E. Ma, *Appl. Phys. Lett.* 83 (2003) 3165.
- [48] Y.M. Wang, E. Ma, *Acta Mater.* 52 (2004) 1699.
- [49] A.A. Elmoustata, M.F. Tambwe, D.S. Stone, *MRS Symp. Proc.* 750 (2003) Y8.14.1.
- [50] Y.M. Wang, E. Ma, *Acta Mater.* (2004) Submitted for publication.
- [51] T.R. Malow, C.C. Koch, P.Q. Miraglia, K.L. Murty, *Mater. Sci. Eng. A* 252 (1998) 36.
- [52] Q. Wei, T. Jiao, K.T. Ramesh, E. Ma, *Scr. Mater.* 50 (2004) 359.
- [53] D. Jang, M. Atzmon, *J. Appl. Phys.* 93 (2003) 9282.
- [54] R. Becker, *Phys. Z.* 26 (1925) 919 (from Ref. [11]).
- [55] M.J. Kobrinski, C.V. Thompson, *Acta Mater.* 48 (2000) 625.
- [56] F.H. Dalla Torre, E.V. Pereloma, C.H.J. Davies, *Scr. Mater.* 51 (2004) 367.
- [57] L.P. Kubin, B. Devincre, M. Tang, *J. Comp. Aided Mater. Des.* 5 (1998) 31.
- [58] Z. Budrovic, H. Van Swygenhoven, P.M. Derlet, S. Van Petegem, M. Schmitt, *Science* 304 (2004) 273.
- [59] V.N. Perevezentsev, V.V. Rybin, V.N. Chuvil'deev, *Acta Metal. Mater.* 40 (1992) 895.
- [60] H. Conrad, J. Narayan, *Scr. Mater.* 42 (2000) 1025.
- [61] Van Swygenhoven, Caro A., *Phys. Rev. B* 58 (1998) 11246.
- [62] Van Swygenhoven, M. Spaczer, A. Caro, D. Farkas, *Phys. Rev. B* 60 (1999) 22.
- [63] H. Conrad, *Mater. Sci. Eng. A* 341 (2003) 216.
- [64] J.C.M. Li, *Trans. AIME* 227 (1963) 239.
- [65] J.P. Hirth, *Metal. Trans.* 3 (1972) 3047.
- [66] A.H.W. Ngan, M. Wen, *Comput. Mater. Sci.* 23 (2002) 139.
- [67] M. Tang, B. Devincre, L.P. Kubin, *Model. Simul. Mater. Sci. Eng.* 7 (1999) 893.
- [68] T.R. Malow, C.C. Koch, *Metal. Mater. Trans. A* 29 (1998) 2285.
- [69] T.R. Malow, C.C. Koch, *Acta Mater.* 46 (1998) 6459.
- [70] J.E. Carsley, W.W. Milligan, S.A. Hackney, E. Aifantis, *Metal. Mater. Trans. A* 26 (1995) 2479.
- [71] J.E. Carsley, A. Fisher, W.W. Milligan, E. Aifantis, *Metal. Mater. Trans. A* 29 (1998) 2261.
- [72] A.W. Thompson, *Acta Metal.* 25 (1977) 83.
- [73] A.M. Lennon, K.T. Ramesh, *Int. J. Plasticity* 20 (2004) 269.